ChemComm

Accepted Manuscript

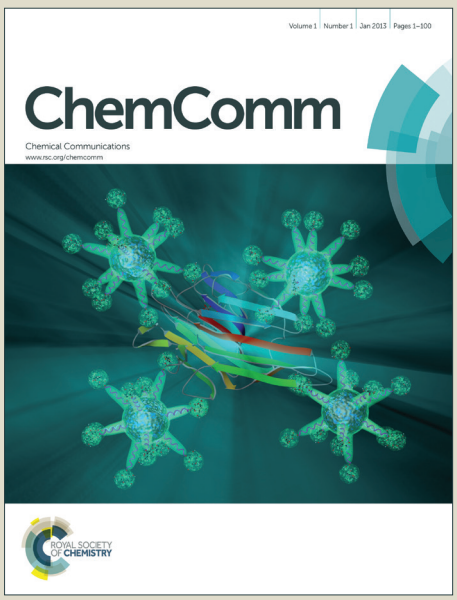

ROYAL SOCIETY OF CHEMISTRY

www.rsc.org/chemcomm

Journal Name

RSCPublishing

COMMUNICATION

Direct White-Light and Dual-channel Barcode Module from Pr(III)-MOF Crystals

Cite this: DOI: 10.1039/x0xx00000x

Bin-Bin Du[a], Yi-Xuan Zhu[a], Mei Pan[a,b]*, Mei-Qin Yue[a], Ya-Jun Hou[a], Kai Wu[a], Lu Yin Zhang[a], Ling Chen[a], Shao-Yun Yin[a], Ya-Nan Fan[a], and Cheng-Yong Su[a,c]*

Received 00th January 2012,
Accepted 00th January 2012

DOI: 10.1039/x0xx00000x

www.rsc.org/

Direct white-light emission and further a dual-channel readable barcode module in both visible and NIR region was established by single-component homo-metallic Pr(III)-MOF crystals for the first time.

Luminescence color modulation and single component white light emitting (SC-WLE) has attracted enormous interest in recent studies of lanthanide coordination complexes, and can be applied in such fields as sensing, imaging, displaying and anti-counterfeiting.[1] Up to now, the common strategies to achieve SC-WLE in Ln^{3+} complexes are dependent on the utilization of mixed-Ln^{3+} metal centers, for example, by the combination of red and green luminescence from Eu^{3+} and Tb^{3+} plus blue emission from the ligand (usually via Gd^{3+} or La^{3+} coordination).[2-4] In a few cases, SC-WLE has also been achieved in homo-metallic Ln^{3+} complexes, such as Sm^{3+}, Eu^{3+}, and Dy^{3+}.[5] However, such observations are still quite rare and deserve further exploration. On the other hand, near-infrared (NIR) emissions from Ln^{3+} ions open the door for much novel and wider applications. Among which, Nd^{3+}, Er^{3+}, and Yb^{3+} complexes have been abundantly reported for their NIR emissions.[6,7] In comparison, the NIR emission from other kinds of Ln^{3+} complexes are scarcely studied.[8] Combining the above two aspects, the exploration of both efficient visible and NIR sensitization as well as direct white luminescence from a single Ln-MOF still remains a challenge.

We report herein a new type of Pr(III)-MOF based on a bipodal zwitterionic ligand. The ligand can sensitize both the visible and NIR emission of Pr^{3+} ions efficiently, and SC-WLE can be achieved in the rarely studied Pr(III)-MOF for the first time. Furthermore, its color tuning via excitation variation provides a dual-channel readable barcode module in both visible and NIR regions.

Complex $[Pr(TMPBPO)_2(NO_3)_3]\cdot C_3H_6O\cdot H_2O$ [**LIFM-17(Pr)**] was prepared by coordination of TMPBPO ligand with $Pr(NO_3)_3\cdot 3H_2O$ in pure water system, and slow diffusion of acetone into the filtrate afforded light green crystals of LIFM-17(Pr) in a yield of 68%. The phase purity of the bulky sample is confirmed by PXRD (powder X-ray diffraction) pattern in comparison with its single-crystal data simulation (Fig. S1). LIFM-17(Pr) crystallizes in the monoclinic space group $P2_1/c$ and the asymmetric unit consists of one Pr^{3+}, two TMPBPO ligands, three coordinated NO_3^- anions and one uncoordinated acetone and water molecules. The Pr^{3+} ion lies in ten-coordination geometry, surrounded by four TMPBPO ligands through O atoms and three NO_3^- anions (Fig. 1). Meanwhile, each bipodal TMPBPO ligand links two Pr^{3+} ions. Among the four TMPBPO ligands around each Pr^{3+} ion, two take *cis*-type configuration and the other two take *trans*-type configuration, thus generating a 2D (4, 4)-MOF as shown in Fig. 1. In the crystal lattice, such (4, 4)-networks are packed in an ABAB fashion in parallel along the *c* direction. TG curve (Fig. S2) confirms rather good thermal stability of LIFM-17(Pr).

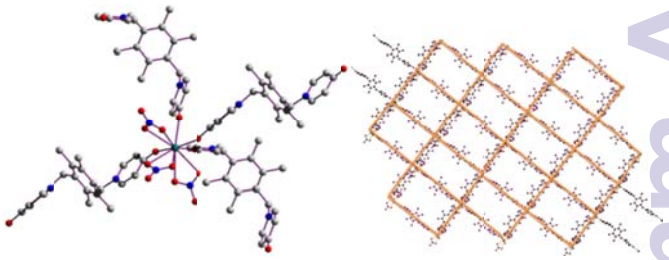

Fig. 1 Crystal structure of complex LIFM-17(Pr). The coordination environment of central Pr^{3+} (left), and the (4, 4) network packing diagram (right). The solvent molecules and hydrogen atoms are omitted for clarity (teal for Pr, blue for N, red for O, and gray for C atoms, respectively).

Solid state UV-Vis absorption and excitation/emission spectra for pure TMPBPO ligand were measured and shown in Fig. S3. As we can see, TMPBPO has two major absorption peaks at 249 and 2[illegible] nm, which may be dominated by the $\pi\rightarrow\pi^*$ transitions on benzene ring and $n\rightarrow\pi^*$ transitions on pyridine ring, respectively. While the excitation band of TMPBPO extends to up to 500 nm, which may be due to the intraligand charge transfer (ILCT) between the central benzene and the terminal pyridine rings.[9] At the excitation of 300 n[illegible]

TMPBPO emits weak and wide luminescence covering 400 to 650 nm, while the excitation at 335 nm affords two salient peaks centering at 415 and 510 nm with similar decay lifetimes of 6.2 and 5.5 ns, typical of intraligand transitions. DFT calculation was also performed with Gaussian 09 software to optimize the geometrical configuration and determine the energy states of TMPBPO ligand using B3LYP method and 6-31G* basis set for atoms C, H, O, and N. As shown in Fig. S4, the optimized geometry of TMPBPO supports the keto-formation, in which the two terminal C-O bond lengths are 1.234 Å, representative of C=O double bond (~120 pm) rather than C-O single bond (~143 pm). From Fig. S4, we can also see that the free ligand takes a *trans*-configuration, in which the two pyridone arms are pointing to the opposite direction of the central benzene ring. Furthermore, the molecule has rather spatially-separated HOMO and LUMO orbitals, with the former dominated by π orbitals from the pyridone terminals, and the latter mainly contributed by π* orbitals from the central benzene ring. This suggests that ILCT (intraligand charge transfer) can happen between the frontier orbitals of TMPBPO, and this wide ILCT excited states might serve as efficient energy reservoirs to sensitize the emission of Pr^{3+} ions, besides the normal ligand-based triplet state, which was estimated to be around 21,500 cm^{-1} by the phosphorescence spectrum of TMPBPO-Gd-MOF (LIFM-19(Gd)) measured at 77 K (Fig. S5). Since the phosphorescence of LIFM-19(Gd) also features in wide band emission (covering 400 to 700 nm), similar to the ILCT-related luminescence of TMPBPO ligand, we can anticipate a synergetic Antenna effect from very broad ILCT and triplet energy levels suitable for versatile and multichannel energy transfer to Pr^{3+} ions.

The relative energy levels and energy transfer pathways for Pr(III)-MOF from TMPBPO ligand are illustrated in Scheme 1. The ligand TMPBPO absorbs UV light to transit from singlet ground (S_0) to the singlet $^1S_1$ or $^1S_2$ states, which further brings forward to a broad triplet state ($^3T^*$). Simultaneously, fast intraligand charge transfer process happens between pyridone and benzene rings, which leads to ILCT states with lower and wider energy levels. The $^3T^*$ and ILCT excited states of TMPBPO ligand are located in the energy levels between 17,000 to 25,000 cm^{-1}, which are suitable for energy transfer to Pr^{3+} ions and therefore, can efficiently sensitize the f-f emissions of Pr^{3+} in both visible and NIR regions.

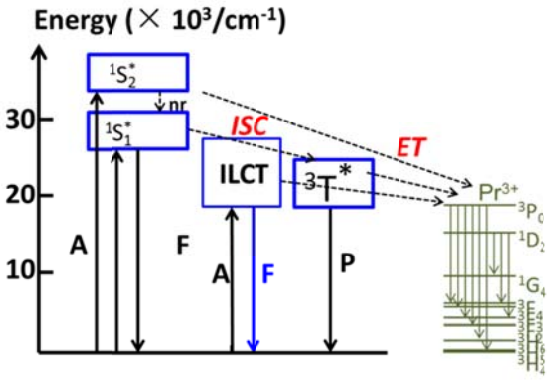

Scheme 1. Diagram for the energy levels and energy transfer pathways in TMPBPO-sensitized visible and NIR emitting Pr(III)-MOF. A, absorption; F, fluorescence; P, phosphorescence; S, singlet; T, triplet; ILCT, intra-ligand charge transfer; ET, energy transfer; ISC, intersystem crossing. Back transfer processes are not drawn for the sake of clarity.

As shown in Fig. 2, in visible region, LIFM-17(Pr) presents several peaks at 480, 550, 590, 620, 650 and 690 nm, which are due to the f-f transitions of $^3P_0 \rightarrow {}^3H_4$, $^3P_0 \rightarrow {}^3H_5$, $^3P_0 \rightarrow {}^3H_6$, $^3P_0 \rightarrow {}^3F_2$, $^3P_0 \rightarrow {}^3F_3$, and $^3P_0 \rightarrow {}^3F_4$ of Pr^{3+}, respectively. The luminescence decay lifetime was detected at the maximum peak of 620 nm, giving a value of 173 μs. In addition to the visible emissions described above, efficient NIR emission bands centering around 850, 1020 and 1470 nm are also generated in LIFM-17(Pr), assignable to f-f transitions from $^1D_2$ emitting level of Pr^{3+} to $^3F_2$, $^3F_4$ and $^1G_4$ ground state, respectively. The decay lifetime detected at 1020 nm at room temperature is 3.8 μs. This large discrepancy in the decay lifetime of visible and NIR emissions manifests that they are originated from different excited states.[10]

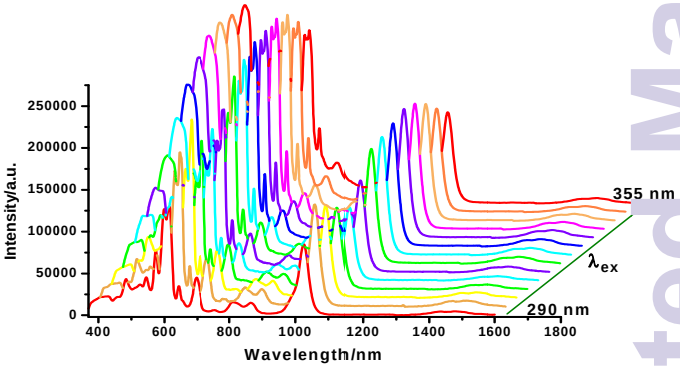

Fig. 2 Full luminescence spectra of LIFM-17(Pr) by varying excitation wavelength from 290 to 355 nm with interval of 5 nm (r. t.).

An unprecedented finding is that LIFM-17(Pr) can generate direct white light and tunable emissions upon the variation of excitation wavelength. As shown in Fig. 3, when varying the excitation from 295 to 315 nm, LIFM-17(Pr) mainly emits the characteristic f-f transition emissions of Pr^{3+}. This means that upon high energy excitation, total energy transfer happens from ligand TMPBPO to Pr^{3+} center. For example, at the excitation of 295 nm, a CIE coordinate of (0.55, 0.37) is achieved, falling into the orange light region. In contrast, at the excitation from 320 to 340 nm, in addition to the Pr^{3+} peak emissions, two broad bands covering 400-450 and 450-600 nm appear, which are assignable to the reserved ILCT emission from the TMPBPO ligand while somewhat affected by f-f transitions of Pr^{3+}. Such incomplete ligand-to-metal energy transfer results in direct white light emission by LIFM-17(Pr) with dual contributions from the metal-based f-f emission and ligand-based ILCT emission. Especially, at the excitation of 335 nm, a CIE coordinate at (0.36, 0.35) can be obtained, affording pure white light to the naked eye and offering one of the rare examples to achieve SC-WLE from single-component and homo-metallic Ln^{3+} complexes. Further lowering the energy of excitation to 345-365 nm, the ILCT emission from TMPBPO ligand gradually dominate the luminescence spectra, and the characteristic f-f transitions of Pr^{3+} becomes barely detected. At the excitation of 365 nm, the CIE coordinate is about (0.27, 0.46). Therefore, bluish–green light is produced. The emitting intensity and brightness with different colors in the visible

region is good enough to be detected clearly by naked eye (as shown by the photos in Fig. 3b), therefore can be applied in such applications as barcode module, which will be discussed below. It should also be noted here that for the ligand-centered emission observed at longer-wavelength excitation (320-365 nm), the contour of the emission peaks are greatly affected by both the f-f absorptions and emissions of Pr^{3+}. For example, the sharp coves formed between 430 to 500 nm are actually attenuated by the super-sensitized f-f absorptions of Pr^{3+} as shown in Fig. S6. This observation is in agreement with the proposed energy transfer pathway from ILCT excited states to the accepting f-levels of Pr^{3+} as discussed above.

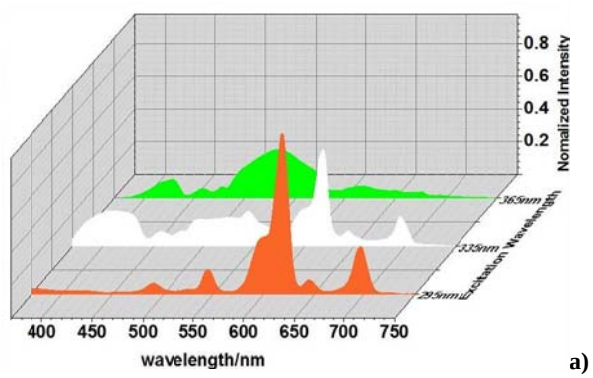

a)

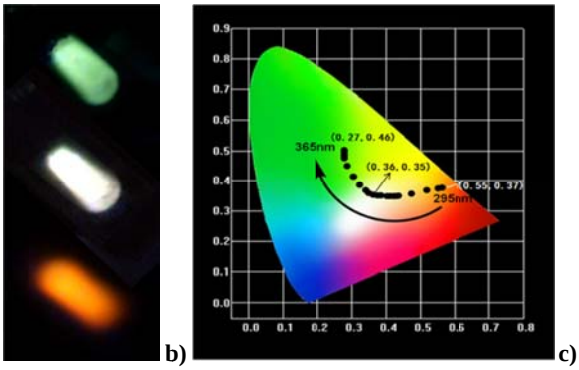

b) c)

Fig. 3 White light and tunable emission of LIFM-17(Pr) in the visible region detected at room temperature. (a) Emission spectra, and (b) photograph at the excitation wavelength of 295 (orange), 335 (white) and 365 (green) nm, respectively. (c) CIE coordinates of the emission spectra at the excitation wavelengths from 295 to 365 nm (the excitation wavelength interval is 5 nm).

The tunable emission of LIFM-17(Pr) in both visible and NIR regions can be further utilized to design a two-channel readable barcode module as shown in Fig. 4. From the full luminescence spectra of LIFM-17(Pr) recorded with steady changing excitation wavelength from 290 to 355 nm (Fig. 2), we can see that the intensity of the ligand-based emissions around 415 and 520 nm are increased gradually, while the Pr^{3+}-based emissions in visible (615 nm) and NIR (1025 nm) region show the opposite decreasing or irregularly changing tendency. The quantitative intensity changes in these four emissions with respect to the variations of excitation wavelengths are shown in Fig. 4a. Based on this emission-excitation variation dependence, an encoding strategy by the means of correlating two encode elements, i.e. emission intensity (or emission integration) vs. excitation wavelength, could be easily established.

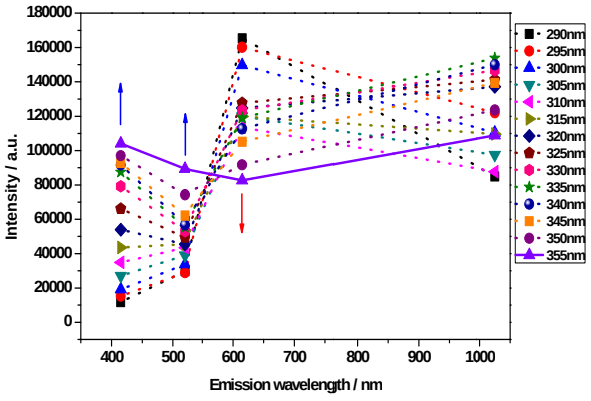

a)

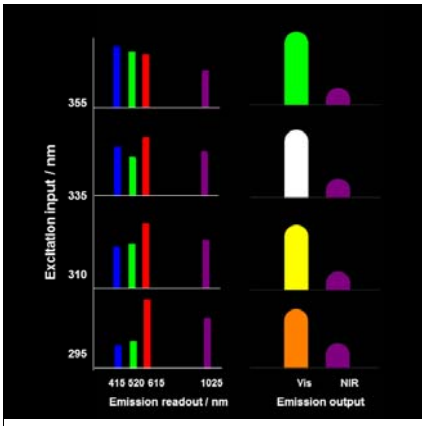

b)

Fig. 4 Demonstration of using tunable emissions of LIFM-17(Pr) as a two-channel readable barcode module. (a) Luminescence intensity changes of the emissions at 415, 520, 615 and 1025 nm in dependence on variations of the excitation wavelengths. (b) Two types of color-coded schematic barcode readout fashions integrating both visible and invisible information.

Interpretation of the encryption information may be achieved in two fashions: (a) monitoring the emission readout at individual emission peaks for comparison of the intensity relationship, and (b) checking the color output based the overall emission integration in the visible region in combination with the invisible NIR readout information. Firstly, the emission intensities at 415, 520, 615 and 1025 excited at 295, 310, 335 and 355 nm were monitored, and then translated into the striped barcode as shown in Fig. 4b left. Furthermore, as described above, the changes of luminescence color from LIFM-17(Pr) in the visible region can be directly detected by naked eye. Therefore, we can design a color-coded barcode module based on four selected sets of data as demonstrated in Fig. 4b right. The overall emission in both visible (350-800 nm) and NIR (800-1600 nm) region when excited at 295, 310, 335 and 355 nm were integrated separately. Using the integration area as the relative longitudinal magnitude, the different emitting color specifying the emission in visible region, and the virtual purple color representing the emission in NIR region (since it is invisible), a schematic barcode graph can be obtained. In which, part of the encoded information is visible, and the overall visual readout changes from orange to yellow, white, and finally green by varying excitation wavelength input. Moreover, by adding another encryption code in NIR region, we actually incorporate additional invisible encoding information for more professional-type readout, which can be

monitored only spectroscopically. Therefore, a dual-channel readable barcode module could be created by using LIFM-17(Pr) as simple single-component and homo-metallic complex luminescent material, which might find potential applications in high encryption technique for anti-counterfeit technology and true-or-false identification for senior security bills, vouchers, certificates, and so on.[11]

In summary, both visible and near infrared emissions are highly sensitized in Pr(III)-MOF crystals from TMPBPO ligand possessing broad ILCT and triplet energy levels. Especially, efficient single component white light can be obtained in the homo-metallic Pr(III)-MOF, and a dual-channel readable barcode module is designed according to the tunable emission of Pr(III)-MOF in both visible and NIR regions, which offers a new approach to synthesize demanding Ln-MOFs with good and applicable luminescent performance.

We thank the 973 Program of China (2012CB821701), NSFC (91222201, 21373276), FRF for the Central Universities (15lgzd05), RFDP of Higher Education of China (20120171130006), and Science and Technology Planning Project of Guangzhou for funding.

Notes and references

[a] MOE Laboratory of Bioinorganic and Synthetic Chemistry, State Key Laboratory of Optoelectronic Materials and Technologies, Lehn Institute of Functional Materials, School of Chemistry and Chemical Engineering, Sun Yat-Sen University, Guangzhou 510275, China
panm@mail.sysu.edu.cn; cesscy@mail.sysu.edu.cn
[b] State Key Laboratory of Structural Chemistry, Fujian Institute of Research on the Structure of Matter, Chinese Academy of Sciences, Fuzhou 350002, China
[c] State Key Laboratory of Applied Organic Chemistry, Lanzhou University, Lanzhou 730000, China
Electronic Supplementary Information (ESI) available: [PXRD, TG, absorption and luminescence spectra, experimental, theoretical and crystallographic information]. See DOI: 10.1039/b000000x/.

1 (*a*) P. Coppo, M. Duati, V. N. Kozhevnikov, J. W. Hofstraat and L. De Cola, *Angew. Chem. Int. Ed.*, 2005, **44**, 1806; (*b*) D. Sykes, I. S. Tidmarsh, A. Barbieri, I. V. Sazanovich, J. A. Weinstein and M. D. Ward, *Inorg. Chem.*, 2011, **50**, 11323; (*c*) Y. Liu, M. Pan, Q.-Y. Yang, L. Fu, K. Li, S.-C. Wei and C.-Y. Su, *Chem. Mater.*, 2012, **24**, 1954; (*d*) H.-B. Xu, X.-M. Chen, Q.-S. Zhang, L.-Y. Zhang and Z.-N. Chen, *Chem. Commun.*, 2009, 7318; (*e*) C.-Y. Sun, X.-L. Wang, X. Zhang, C. Qin, P. Li, Z.-M. Su, D.-X. Zhu, G.-G. Shan, K.-Z. Shao, H. Wu and J. Li, *Nat. Commun.*, 2013, **4**, 2717; (*f*) Q.-Y., Yang, M. Pan, S.-C. Wei, K. Li, B.-B. Du, C.-Y. Su, *Inorg. Chem.*, 2015, **54**, 5707.

2 (*a*) H. Zhang, X. Shan, L. Zhou, P. Lin, R. Li, E. Ma, X. Guo and S. Du, *J. Mater. Chem. C*, 2013, **1**, 888; (*b*) Z.-F. Liu, M.-F. Wu, S.-H. Wang, F.-K. Zheng, G.-E. Wang, J. Chen, Y. Xiao, A-Q. Wu, G.-C. Guo and J.-S. Huang, *J. Mater. Chem. C*, 2013, **1**, 4634; (*c*) S.-L. Zhong, R. Xu, L.-F. Zhang, W.-G. Qu, G.-Q. Gao, X.-L. Wu and A.-W. Xu, *J. Mater. Chem.*, 2011, **21**, 16574; (*d*) X. Rao, Q. Huang, X. Yang, Y. Cui, Y. Yang, C. Wu, B. Chen, and G. Qian, *J. Mater. Chem.*, 2012, **22**, 3210; (*e*) M.-L. Ma, C. Ji and S.-Q. Zang, *Dalton Trans.*, 2013, **42**, 10579.

3 (*a*) N. Kerbellec, D. Kustaryono, V. Haquin, M. Etienne, C. Daiguebonne and O. Guillou, *Inorg. Chem.*, 2009, **48**, 2837; (*b*) A. R. Ramya, S. Varughese and M. L. P. Reddy, *Dalton Trans.*, 2014, **43**, 10940; (*c*) L. L. da Luz, B. F. L. Viana, G. C. O. da Silva, C. [illegible] Gatto, A. M. Fontes, M. Malta, I. T. Weber, M. O. Rodrigues and S. A. Júniora, *CrystEngComm*, 2014, **16**, 6914; (*d*) S.-M. Li, X.-[illegible] Zheng, D.-Q. Yuan, A. Ablet and L.-P. Jin, *Inorg. Chem.*, 2012, **51**, 1201; (*e*) Q. Tang, S. Liu, Y. Liu, D. He, J. Miao, X. Wang, Y. Ji [illegible] Z. Zheng, *Inorg. Chem.*, 2014, **53**, 289.

4 (*a*) F. Zhang, P. Yan, H. Li, X. Zou, G. Hou, G. Li, *Dalton Trans.*, 2014, **43**, 12574; (*b*) H. Zhang, X. Shan, Z. Ma, L. Zhou, M. Zhan[illegible], P. Lin, S. Hu, E. Ma, R. Li, S. Du, *J. Mater. Chem. C*, 2014, **2**, 1367; (*c*) M.-L. Ma, J.-H. Qin, C. Ji, H. Xu, R. Wang, B.-J. Li, S.-Q. Zan[illegible], H.-W. Hou, S. R. Batten, *J. Mater. Chem. C*, 2014, **2**, 1085.

5 (*a*) G. J. He, D. Guo, C. He, X. L. Zhang, X. W. Zhao and C. Y. Dua[illegible], *Angew. Chem., Int. Ed.*, 2009, **48**, 6132; (*b*) Y.-H. Zhang, X. Li and S. Song, *Chem. Commun.*, 2013, **49**, 10397; (*c*) Q.-Y. Yang, K. Wu, J.-[illegible] Jiang, C.-W. Hsu, M. Pan, J.-M. Lehn and C.-Y. Su, *Chem. Commun.*, 2014, **50**, 7702.

6 (*a*) J. An, C. M. Shade, D. A. Chengelis-Czegan, S. Petoud, N. [illegible] Rosi, *J. Am. Chem. Soc.*, 2011, **133**, 1220; (*b*) D. J. Lewis, P. B. Glover, M. C. Solomons, and Z. Pikramenou, *J. Am. Chem. Soc.*, 2011, **133**, 1033; (*c*) A. de Bettencourt-Dias, P. S. Barber, and S. Bauer, *J. Am. Chem. Soc.*, 2012, **134**, 6987.

7 (*a*) L. Sun, Y. Qiu, T. Liu, H. Peng, W. Deng, Z. Wang, and L. Shi, *RSC Adv.*, 2013, **3**, 26367; (*b*) J. Zhang, P. D. Badger, S. J. Geib, [illegible] S. Petoud, *Angew. Chem. Int. Ed.*, 2005, **44**, 2508; (*c*) J. Jankolovi[illegible] C. M. Andolina, F. W. Kampf, K. N. Raymond, and V. L. Pecoraro, *Angew. Chem. Int. Ed.*, 2011, **50**, 9660.

8 (*a*) M. D. Ward, *Coord. Chem. Rev.*, 2007, **251**, 1663; (*b*) X. Yang, D. Schipper, R. A. Jones, L. A. Lytwak, B. J. Holliday, and S. Huang, *J. Am. Chem. Soc.*, 2013, **135**, 8468; (*c*) S. Dang, X. Min, W. Yang, F.-Y. Yi, [illegible] You, and Z.-M. Sun, *Chem. Eur. J.*, 2013, **19**, 17172; (*d*) L. Sun, Y. Qi[illegible] T. Liu, J. Z. Zhang, S. Dang, J. Feng, Z. Wang, H. Zhang, and L. Sh[illegible] *ACS Appl. Mater. Interfaces*, 2013, **5**, 9585.

9 (*a*) S. Comby, D. Imbert, C. Vandevyver, and J.-C. G. Bünzli, *Chem. Eur. J.*, 2007, **13**, 936; (*b*) W.-K. Wong, X. Zhu, W.-Y. Wong, *Coord. Chem. Rev.*, 2007, **251**, 2386; (*c*) X. Zhu,. W.-K. Wong, W.-Y. Wong, and X. Yang, *Eur. J. Inorg. Chem.*, 2011, 4651; (*d*) M. V. López, S. V. Eliseev, J. M. Blanco, G. Rama, M. R. Bermejo, M. E. Vázquez, and J.-C. G. Bünzli, *Eur. J. Inorg. Chem.*, 2010, 4532.

10 (*a*) Q.-X. Yao, Z.-F. Ju, W. Li, W. Wu, S.-T. Zheng, J. Zhang, *CrystEngComm*, 2008, **10**, 1299; (*b*) M. Higuchi, D. Tanaka, S. Horike, H. Sakamoto, K. Nakamura, Y. Takashima, Y. Hijikata, N. Yanai, J. Kim, K. Kato, Y. Kubota, M. Takata and S. Kitagawa, *J. Am. Chem. Soc.*, 2009, **131**, 10336; (*c*) Q.-X. Yao, Z.-F. Ju, X.-H. Ji, J. Zhang, *Inorg. Chem.*, 2009, **48**, 1266.

11 (*a*) Z. Ahmed, K. Iftikhar, *J. Phys. Chem. A*, 2013, **117**, 11183; (*b*) [illegible] D. Regulacio, M. H. Pablico, J. A. Vasquez, P. N. Myers, S. Gentry, M. Prushan, S.-W. Tam-Chang, S. L. Stoll, *Inorg. Chem.*, 2008, **47**, 1512; (*c*) E. G. Moore, G. Szigethy, J. Xu, L.-O. Pålsson, A. Beeby, K. N. Raymond, *Angew. Chem. Int. Ed.*, 2008, **47**, 9500; (*d*) K. [illegible] White, D. A. Chengelis, K. A. Gogick, J. Stehman, N. L. Rosi, and S. Petoud, *J. Am. Chem. Soc.*, 2009, **131**, 18069.

